JACS
JOURNAL OF THE AMERICAN CHEMICAL SOCIETY

ARTICLE

pubs.acs.org/JACS

Synthesis and Characterization of Single-Layer Silver−Decanethiolate Lamellar Crystals

Liang Hu,[†] Lito P. de la Rama,[†] Mikhail Y. Efremov,[‡] Yonathan Anahory,[§] Francois Schiettekatte,[§] and Leslie H. Allen*[,†]

[†]Department of Materials Science and Engineering, Coordinated Science Laboratory, University of Illinois at Urbana−Champaign, Urbana, Illinois 61801, United States

[‡]Department of Chemical and Biological Engineering and Center for Nanotechnology, University of Wisconsin−Madison, Madison, Wisconsin 53706, United States

[§]Regroupement Québecois sur les matériaux de pointes (RQMP), Département de physique, Université de Montéal, Montréal, Québec, Canada H3C 3J7

ABSTRACT: We report the synthesis of silver−decanethiolate (AgSC10) lamellar crystals. Nanometer-sized Ag clusters grown on inert substrates react with decanethiol vapor to form multilayer AgSC10 lamellar crystals with both layer-by-layer and in-plane ordering. The crystals have strong (010) texture with the layers parallel to the substrates. The synthesis method allows for a precise control of the number of layers. The thickness of the lamellae can be manipulated and systematically reduced to a single layer by decreasing the amount of Ag and lowering the annealing temperature. The single-layer AgSC10 lamellae are two-dimensional crystals and have uniform thickness and in-plane ordering. These samples were characterized with nanocalorimetry, atomic force microscopy (AFM), transmission electron microscopy (TEM), X-ray diffraction (XRD), X-ray reflectivity (XRR), Fourier transform infrared spectroscopy (FTIR), and Rutherford backscattering spectroscopy (RBS).

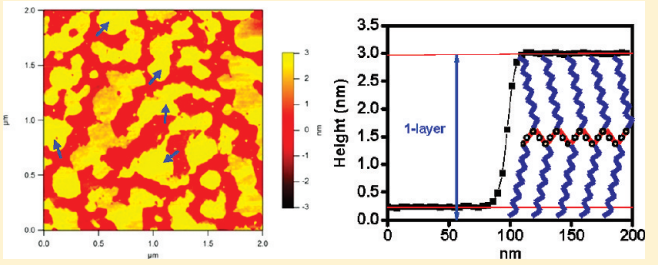

1. INTRODUCTION

Unique underlying intrinsic chemical and physical properties of materials allow us to synthesize special sizes and shapes of materials. Examples in nature where special "magic" number sizes are favored include metallic and metal−organic clusters[1−4] as well as materials with special shapes such as two-dimensional (2D) crystals of graphene.[5]

Self-assembly of organic molecules with metals provides an exciting chemical synthesis path to systematically create these special sized and shaped materials. These new synthesis methods are already fostering new potential applications in the areas such as nanoelectronics,[6] luminescence,[7−9] biocompatible surfaces,[10] and interfacial toughening.[11]

Reaction between alkanethiols and metals forms one of the most extensively studied self-assembly systems. Two specific reaction products are addressed in this work: alkanethiol-monolayer-protected Ag clusters (MPCs) and silver−alkanethiolate (AgSR, R = C_nH_{2n+1}). MPCs and AgSR consist of the same elements but are different in stoichiometry and physical shape. MPCs have relatively high Ag content and a convex shape, whereas AgSR has a planar lamellar shape and unity stoichiometric ratio between Ag and S. The main thermodynamic driving forces for the self-assembly process include the bonding between metal and S and the van der Waals interaction between alkyl chains.[12,13] Both MPCs and AgSR may be simultaneously present during the intermediate stages of formation. Both species may act as a precursor for each other.[14−16]

MPCs with special sizes have been produced; for example, "magic-sized" MPCs with exactly 102 gold atoms have been recently synthesized.[3] In this work we use this material system to produce special shapes and sizes of stacked-layered polymeric AgSR including single-layer 2D crystals of AgSR.

Two-dimensional self-assembled monolayers (SAMs) with ordered arrangement are observed on nominally planar metal surface,[12,17,18] although the interfacial structures remain controversial.[19] Recent experimental and theoretical studies proposed new models for the interfacial structure: metal−thiolate complexes and polymeric metal thiolate.[20−23] AgSR can be conceptually constructed as two layers of 2D SAMs stacked back to back.

MPCs can be considered as a metallic core with a metal−thiolate complex shell.[3,24,25] If the size of the metal cluster is large the properties of the MPC approach those of the 2D SAMs. If the size of the metallic core is reduced to a lower limit, then all of the metal atoms in the cluster are directly bonded to S.[26,27] For long-chain molecules, in the case where stoichiometry is 1.0, alternative structures to the MPCs may be thermodynamically favorable such as polymeric metal−thiolate complexes.

Received: August 31, 2010
Published: March 03, 2011

dx.doi.org/10.1021/ja107817x | J. Am. Chem. Soc. 2011, 133, 4367–4376

Metal−thiolates have multilayer structure, and each layer has a planar polymeric structure of −(metal−S)− network as the central plane (backbone).[28−35]

In our prior work, we developed a new method which generates two phases on inert surfaces—MPCs and AgSR.[16] We deposited Ag onto inert substrates via thermal evaporation which then reacted with alkanethiol solution. Large clusters were coated with alkanethiol and formed MPCs, whereas small clusters were more likely to transform into AgSR.

In this work we modify the synthesis method in order to achieve only the AgSR phase as the reaction product. Extremely small Ag clusters form on inert surfaces and then react with alkanethiol vapor[36] instead of liquid immersion. The thickness (the number of layers) of the formed AgSR lamellar crystals can be controlled by adjusting the amount of Ag and the annealing schedule. This synthesis method allows for a precise control on the number of layers in AgSR lamellar crystals.

By limiting the average thickness of Ag to 0.1 nm, we obtain 2D crystals consisting of single-layer AgSR which is the ultimate lower limit to a 3D crystal form. Two-dimensional crystals hold a special place in nature. Until recently with the discovery of graphene in 2004, conventional wisdom held that a 2D crystal is thermodynamically unstable because of the reduced melting temperature of material at the nanometer scale—size-dependent melting.[5] From the technological standpoint the 2D crystal is the basic building block for self-assembly. It is where bottom-up assembly has its natural starting point. Here we describe the smallest unit of AgSR lamellar crystal—a single-layer 2D crystal. This crystal is nearly free-standing having a free surface at the top while the bottom interface with an inert substrate has extremely small interface energy.

In addition, when combined with the capability of changing the chain length, functionality of the headgroup, and metal type (Au, Ag, Cu, etc.), this synthesis method provides a new platform for probing a wide spectrum of materials properties at the nanometer size range.

2. EXPERIMENTAL SECTION

2.1. Sample Preparation. *2.1.1. Materials.* Silver pellets (99.99%, Kurt J. Lesker Co.) are used as vapor deposition sources. 1-Decanethiol ($C_{10}H_{21}SH$) is obtained from Sigma-Aldrich Co. and used as received.

2.1.2. Synthesis. We deposit Ag thin film onto inert substrates via thermal evaporation with the base pressure of 5×10^{-8} Torr. By depositing 0.06−0.6 nm thick Ag film, we obtain Ag clusters on the substrate surface. The samples are then placed in contact with the saturated decanethiol vapor at room temperature for 96 h. After the reaction, the samples are thermally annealed in vacuum (10^{-7} Torr) for 2 h. The heating rate is less than 10 °C/h, and the cooling rate is less than 15 °C/h.

Two parameters are critical to the crystal size of the final product: (1) the amount of deposited Ag, and (2) the annealing temperature (T_{Ann}). We use the average thickness (l_{Ag}) of the deposited film as a convenient measure for the amount of Ag on surfaces.

2.1.3. Substrates. The type of the substrate is determined by the instrumental technique used for the sample characterization. All of the substrates used here have inert surfaces. (1) The substrate in nanocalorimetry sensors is low-residual-stress SiN_x membrane. Since both nanocalorimetry and Rutherford backscattering spectroscopy (RBS) are used to estimate the amount of sample, both measurements are performed on the samples prepared directly on the nanocalorimetry sensors. In addition, double-side polished Si wafers coated with low-residual-stress SiN_x film are used for Fourier transform infrared spectroscopy (FTIR) study. (2) Double-side polished Si wafers with native oxide have the advantage of low surface roughness and are used for atomic force microscopy (AFM) and X-ray studies to improve the accuracy of the crystals size measurements. (3) Carbon membranes on copper grids are used in the studies with transmission electron microscopy (TEM) for better imaging contrast.

2.2. Sample Characterization. *2.2.1. Nanocalorimetry.* There are two challenges in the calorimetric study of AgSC10 lamellar crystals on surfaces: (1) the samples are thin (3−75 nm) and have a mass in the nanogram scale (5−50 ng); (2) the size and shape of AgSC10 crystals are sensitive to the thermal treatment prior to the characterization. Due to the miniscule sample size, the calorimetric measurements are performed with nanocalorimetry,[37,38] which has high sensitivity (∼0.1 nJ/K) and ultrafast heating rate (∼50 000 °C/s).[2,39−41] We use sensors with platinum metallization in this study and perform calorimetric measurements in vacuum ($<1 \times 10^{-7}$ Torr). The melting transition is characterized and used to identify the materials on the surfaces. In addition, we obtain the amount of alkanethiolate by measuring the heat capacity of the sample $\Delta C_p(T)$ (T = 150−180 °C) and dividing it with the specific heat of the sample which is assumed to be equal to that of alkane. The uncertainty is about 2 pmol.

2.2.2. X-ray. X-ray diffraction (XRD) and X-ray reflectivity (XRR) studies are carried out on a Philips X'pert diffractometer with Cu Kα (1.5418 Å) radiation. XRD is used to determine the layer spacing in multilayer AgSC10 lamellar crystals and to estimate the average lamellar thickness by using Scherrer analysis. XRR is used to measure the thickness of monodispersed single-layer AgSC10 lamellar crystals on the surface.

2.2.3. Atomic Force Microscopy. An Asylum MFP-3D AFM is used to investigate the topography of AgSC10 lamellar crystals on the substrate surface. Two methods are adopted for measurement of lamellar thickness. First, a histogram of the number of pixels as a function of height is plotted. The first peak in the histogram corresponds to the substrate surface, while the following ones correspond to the top surfaces of the AgSC10 lamellae. Since AgSC10 lamellae are orientated in parallel with the substrate surface, the distances between the substrate peak and the AgSC10 peaks equal the thicknesses of the lamellae which are the products of layer thickness (d) and number of layers (n). The histogram can be used to determine both d and n. Second, the thickness of AgSC10 lamellar crystals can also be obtained by measuring the step height at the edge of the crystals. AFM line scans that cross from the substrate to the top surface of the crystals are randomly selected. The measured step heights are then divided by the layer thickness to obtain the number of layers.

AFM is also used to determine the total volume of AgSC10 crystals on the surface. The density of AgSC10 lamellae can be calculated based on the molecular model in which the alkyl chains are close-packed.[31] Therefore, the average surface concentration of AgSC10 (mol/m^2) can be calculated.

2.2.4. Transmission Electron Microscopy. A JEOL 2010 TEM is used at 200 kV to study samples prepared on holey carbon membranes. Scanning transmission electron microscopy (STEM) mode is used to increase the contrast of imaging.

2.2.5. Rutherford Backscattering Spectroscopy. RBS is performed on the samples prepared on nanocalorimetry sensors with 2 MeV He^+ ion beam. The amount of Ag is obtained by simulation of the experimental spectra.[42]

2.2.6. Fourier Transform Infrared Spectroscopy. A Thermo Nicolet Nexus 670 FTIR is used to study the conformational order of the alkyl chains in AgSC10. Absorbance spectra are taken in the reflection mode with a freshly deposited Au mirror placed on top of samples. The spectral resolution is 1 cm^{-1}. The signal-to-noise ratio is improved by averaging over 128 scans.

3. RESULTS

3.1. Multilayer AgSC10 Lamellar Crystals. We first describe the characterization of multilayer silver−decanethiolate (denoted AgSC10) lamellar crystals (sample M). The experimental parameters (l_{Ag} = 0.63 nm, T_{Ann} = 115 °C) and results are listed in Table 1.

Thermal analysis is an effective method to characterize the phase transition of materials. Thermal properties such as melting point (T_m) and latent heat of fusion (H_m) are useful in identifying and differentiating the phases that compose the reaction product. Nanocalorimetric studies have been reported on different alkanethiolates including 2D SAMs on planar metal surface,[16,43] 3D SAMs in MPCs,[43] and AgSR lamellar crystals grown on surfaces.[16] Thermal analysis of bulk AgSR[29,32,44] and MPCs[45,46] synthesized in a solution has been done using conventional calorimetry. Although the alkyl chains are the primary component attributed to melting, AgSR melts at a much higher temperature (125−140 °C)[29,32,44] than alkyl chain monolayers (45−75 °C).[43,45,46] Therefore, the melting characteristics can be used to distinguish the species of the reaction products. Figure 1a shows the results of C_p measurements. Values for the T_m = 131 ± 2 °C and H_m = 30 ± 5 kJ/mol agree well with the values for bulk AgSC10 (T_m = 132 °C and H_m = 32.4 kJ/mol) obtained using conventional calorimetry.[29,44] Therefore, we deduce that the majority of the reaction product is AgSC10. Only a small amount, if any, of MPC is present since we do not observe a melting transition at lower temperatures (<70 °C).[43,45,46]

Table 1. Experimental Parameters in the Synthesis of a Series of Samples and the Obtained Crystal Sizes

sample	l_{Ag} (nm)[a]	T_{Ann} (°C)[b]	$d_{cluster}$ (nm)[c]	density $(1/\mu m^2)$[d]	n[e]
M	0.63	115	2.9	3.3×10^4	average = 11
N	0.63	20	2.9	3.3×10^4	average = 2.3
A	0.28	105			3, 4, 5
B	0.39	93			2, 3, 4
C	0.22	88			2
D	0.20	81			1, 2
E	0.13	88	1.3	2.3×10^4	1
F	0.14	81			1
G	0.06	59			1

[a] The amount of Ag (l_{Ag}) used in the synthesis. [b] The annealing temperature (T_{Ann}) used in the synthesis. [c] The average Ag cluster size ($d_{cluster}$). [d] The cluster density on the surface. [e] The number of layers in the obtained AgSC10 crystals.

The overall stoichiometric ratio between alkanethiolate and Ag is 0.93 ± 0.17 where the amount of AgSC10 (163 ± 10 pmol) is calculated from ΔC_p values from C_p measurements and the amount of Ag (175 ± 20 pmol) is measured via RBS. We conclude that most of the Ag and alkanethiolate are in the AgSC10 phase where the stoichiometric ratio is equal to unity.

To better understand the structure of the AgSC10 crystals grown on the surface, we use XRD and AFM for further characterization. AgSC10 forms lamella where the lateral dimension (micrometer scale) is much larger than the thickness dimension (nanometer scale). The molecular model of AgSR lamella shows two levels of ordering:[28−31,33,34] (1) layer-by-layer ordering—the formation of multilayer structure; (2) in-plane ordering—the ordered packing of alkyl chains inside each single layer of AgSR crystals.

The XRD diffractogram of sample M (red curve in Figure 1b) clearly shows a series of diffraction peaks attributed to the "lamella reflections" of a multilayered structure. Indexing the diffraction peaks indicates that the layer spacing is 2.99 ± 0.01 nm, which agrees well with the reported values for AgSC10 bulk samples.[34,44] Note that the intensity of the (0k0) diffraction peaks "oscillates": the even numbered peaks ((020), (040), (060), etc.) are weaker than expected as compared to the odd

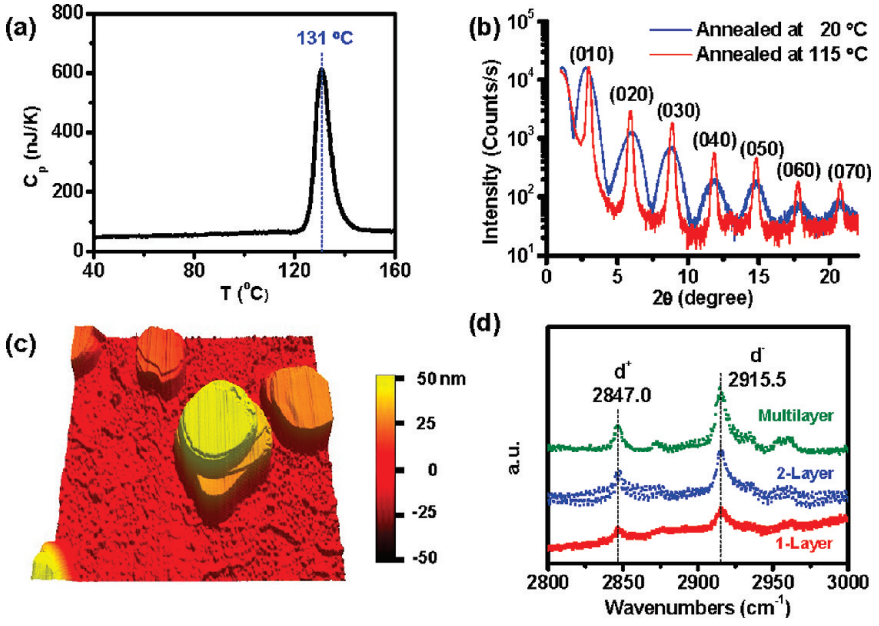

Figure 1. (a) Calorimetric measurement of sample M shows a phase transition at 131 ± 2 °C which is attributed to the melting of AgSC10 crystals; (b) X-ray diffractograms of samples M (red curve) and N (blue curve) which have been annealed at 115 and 20 °C, respectively; (c) AFM micrograph (5 μm × 5 μm) of sample M; (d) FTIR spectra of samples M (green curve), C (blue curve), and E (red curve) which are composed of multilayer, two-layer, and single-layer AgSC10 lamellar crystals.

dx.doi.org/10.1021/ja107817x |J. Am. Chem. Soc. 2011, 133, 4367–4376

numbered peaks ((010), (030), (050), etc.). This intensity oscillation has also been observed on bulk samples[31,44] and is due to the presence of mirror symmetry elements which are perpendicular to the layer stacking direction.[47]

AFM micrographs of sample M also demonstrate the formation of multilayer lamellae which is evidenced by clearly defined steps, as shown in Figure 1c. The AgSC10 crystals have strong (010) texture with layers parallel to the substrate surface. The total thickness of these multilayer lamellae extends up to 75 nm (~25 layers). The average crystal thickness estimated by AFM analysis is equivalent to 8.5 layers, which is close to the value of 11 layers as determined using Scherrer analysis of XRD results.

We note that the AgSC10 phase forms during the reaction between Ag clusters and alkanethiol prior to any subsequent annealing. Thermal annealing only promotes the AgSC10 crystal growth. For comparison, another sample (sample N) is prepared in a similar manner (l_{Ag} = 0.63 nm) as sample M but with a different annealing temperature (T_{Ann} = 20 °C). XRD study (blue curve in Figure 1b) also shows diffraction peaks corresponding to multilayer AgSC10. However, the peaks are much broader as compared to those of sample M, which is expected since the crystals in sample N are smaller. Estimates using Scherrer analysis indicate the average crystal size increases from 2.3 (sample N) to 11 layers (sample M) during annealing.

We note that XRD only shows the lamellar reflections[48] (the layer-by-layer ordering) but does not show diffraction peaks which could be used to determine the structure inside each AgSC10 layer (in-plane ordering). Observable diffraction peaks are absent because the sample is thin (~30 nm on average) and the intensity of the X-ray source is not strong enough. Nevertheless, in-plane ordering can be deduced from AFM micrographs (Figure 1c) which show distinct characteristics of single crystals—straight facets, smooth surfaces, and terraces. These characteristics indicate that the alkyl chains are packed in an ordered structure inside each single layer. In addition, the FTIR spectrum (green curve in Figure 1d) reveals that the symmetric (d+) and antisymmetric (d−) stretching modes of methylene group (CH_2) occur at 2847.0 ± 1.0 and 2915.5 ± 1.0 cm^{-1} and are consistent with those of AgSC10 bulk samples.[34] Since the peak positions are sensitive to the conformational order, we conclude the alkyl chains are fully extended inside the AgSC10 lamellar crystals.

The nanocalorimetry, XRD, AFM, and FTIR results demonstrate that the reaction between Ag clusters and alkanethiol vapor is an effective method to synthesize AgSC10 lamellar crystals. Initially, the crystals are small but can grow into large single crystals during thermal annealing.

3.2. Systematically Reducing Layer Number of AgSC10: Size Control. We synthesize AgSC10 lamellar crystals with progressively smaller thickness, i.e., less number of layers (n), by adjusting two processing parameters: the amount of Ag (l_{Ag}) and the annealing temperature (T_{Ann}). Table 1 describes a series of experiments where we systematically decrease the size of the crystals from 11 layers down to 1 layer.

Figure 2 shows the number of layers for samples A−E using AFM height histograms. For example, in sample A, there is a mixture of three different crystal sizes (three, four, and five layers). In contrast, in sample E only one crystal size (one layer) is present. All of the AFM analysis hereafter has been corrected for artifacts caused by residue (excess alkanethiol) on the substrate, which will be detailed in the Discussion section of the paper. The amount of correction is annotated in each histogram as an offset in the substrate peak.

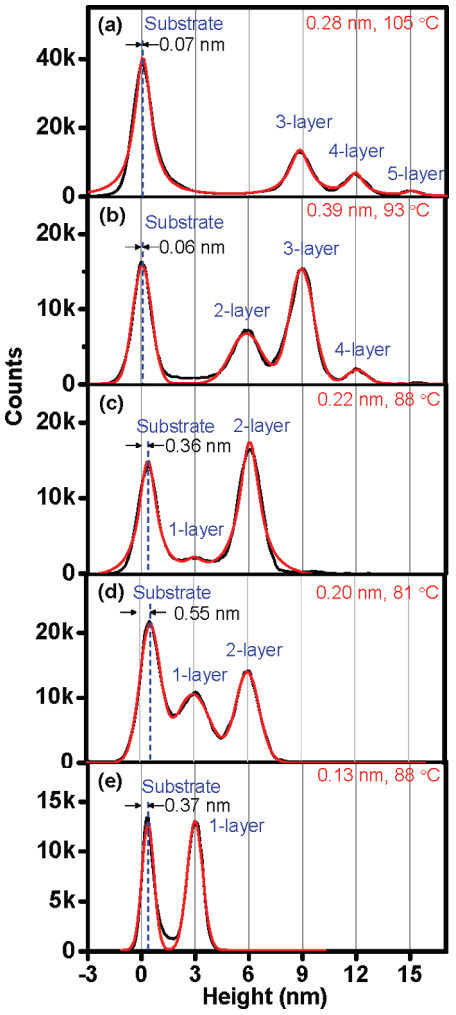

Figure 2. (a−e) AFM height histograms of samples A−E which are synthesized with the same method but different experimental parameters (l_{Ag} and T_{Ann}) as listed in the top-right corner of each histogram. The first peak in each histogram corresponds to the substrate, whereas the others correspond to the AgSC10 lamellar crystals and are labeled with the number of layers. The shifting of the substrate peaks from 0 nm is due to AFM baseline correction.

Control of AgSC10 size (number of layers) is coupled to the control of the initial Ag cluster size and cluster density. The size of Ag clusters is directly related to the amount of Ag deposited onto the surface. Figure 3 compares two as-deposited samples with different amounts of Ag. Figure 3a shows TEM micrograph of sample N (0.63 nm) which has a density of 3.3 × 10^4 clusters/μm^2 with a median diameter ($d_{cluster}$) of 2.9 nm (Figure 3c). In comparison, Figure 3b shows sample E (0.13 nm) with a lower amount of Ag which has a density of 2.3 × 10^4 clusters/μm^2 with a median diameter of 1.3 nm (Figure 3d).

The stoichiometric ratio between alkanethiolate and Ag in the AgSC10 phase is near unity for all samples. The ratio is 1.0 when the amount of Ag is below 0.25 nm and thus all of the Ag is consumed in the reaction forming AgSC10, whereas for larger amounts of Ag the stoichiometry decreases slightly (~0.90). Stoichiometry is determined from the amount of Ag obtained with RBS (Figure 4a) and from the amount of AgSC10 obtained

dx.doi.org/10.1021/ja107817x |J. Am. Chem. Soc. 2011, 133, 4367–4376

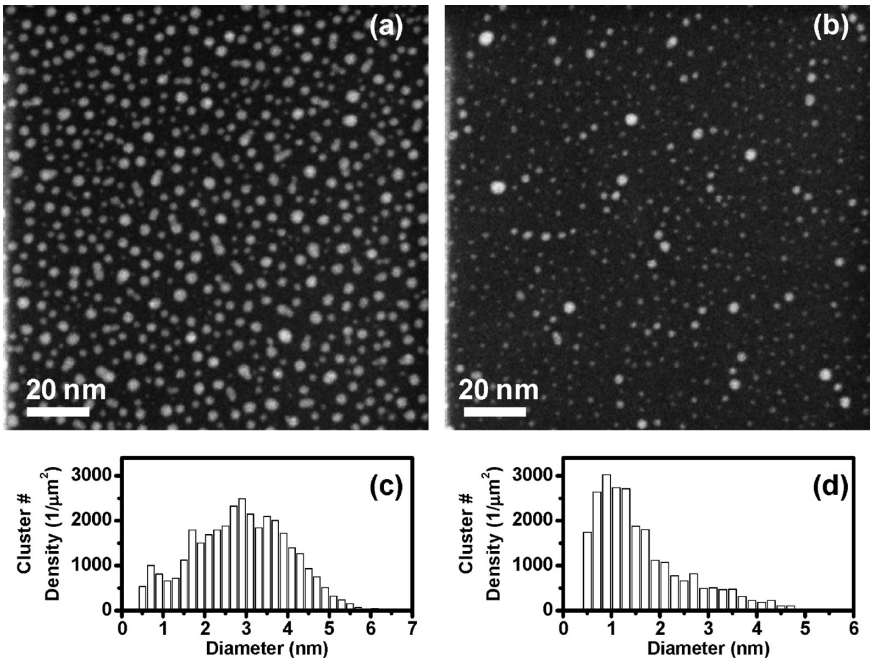

Figure 3. (a and b) TEM micrographs of Ag clusters grown on carbon membranes via vapor deposition. The cluster size and density are determined by the amount of Ag: (a) 0.63 nm; (b) 0.13 nm. (c and d) The histograms of cluster number density corresponding to panels a and b, respectively.

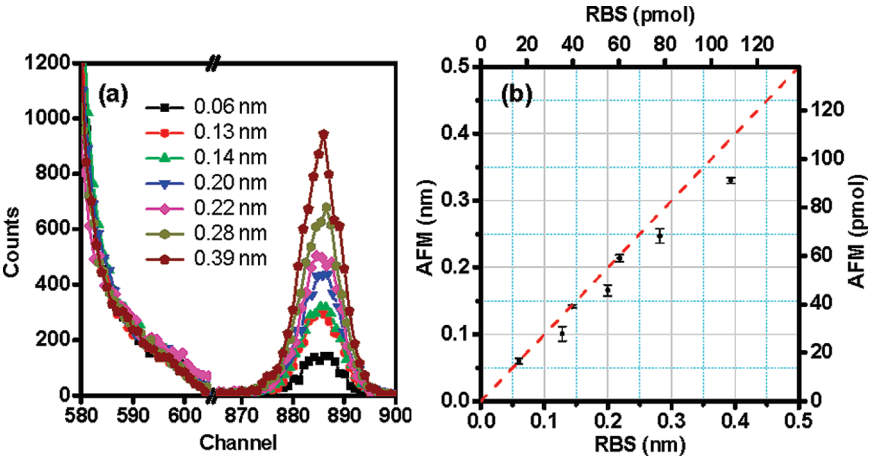

Figure 4. (a) RBS spectra showing the amount of Ag in samples A−G. (b) The amount of AgSC10 measured with AFM vs the amount of Ag measured with RBS. For the convenience of comparison, the quantities are transformed to the equivalent values in the units of nanometer (nm) and picomole (pmol).

from AFM. The stoichiometry of samples A−G is plotted in Figure 4b. For clarity, the values are also plotted in terms of the equivalent uniform thickness of Ag.

3.3. Nearly Monodispersed Two-Layer AgSC10 Lamellar Crystals. The 2D and 3D AFM micrographs of sample C are shown in Figure 5, parts a and b, respectively. The red area corresponds to the substrate surface, whereas the yellow platelets correspond to the AgSC10 crystals which are distributed over the entire surface. The AFM histogram (Figure 2c) indicates that the AgSC10 lamellar crystals have nearly uniform thickness (number of layers), i.e., about 95% of the crystals have two layers, whereas about 5% have one layer. The surface coverage of the two-layer AgSC10 lamellar crystals is about 50% of the entire surface area.

The X-ray diffractogram of sample C is shown in Figure 5c (blue curve) and compared with that of multilayer crystals (red curve, redrawn from Figure 1b). The peak positions are consistent with each other, except that the first peak (010) is slightly shifted toward a lower angle. This shift is a result of the convolution of the X-ray reflectivity and diffraction signals. Layer spacing determined from the (020) and (030) diffraction peaks is 2.98 ± 0.10 nm, which is the same as the layer spacing of the multilayer AgSC10.

The layer spacing of sample C can also be obtained using the AFM height histogram. The difference between the heights of single-layer and two-layer crystals is 3.1 ± 0.1 nm, which is consistent with the XRD layer spacing (2.98 ± 0.10 nm). We can use this differential height analysis method because a few (5%) single-layer crystals are available as an internal height reference. Values for the peak height are shifted by 0.36 nm as shown in Figure 2c. In addition, individual AFM line scans (annotated by

dx.doi.org/10.1021/ja107817x |J. Am. Chem. Soc. 2011, 133, 4367–4376

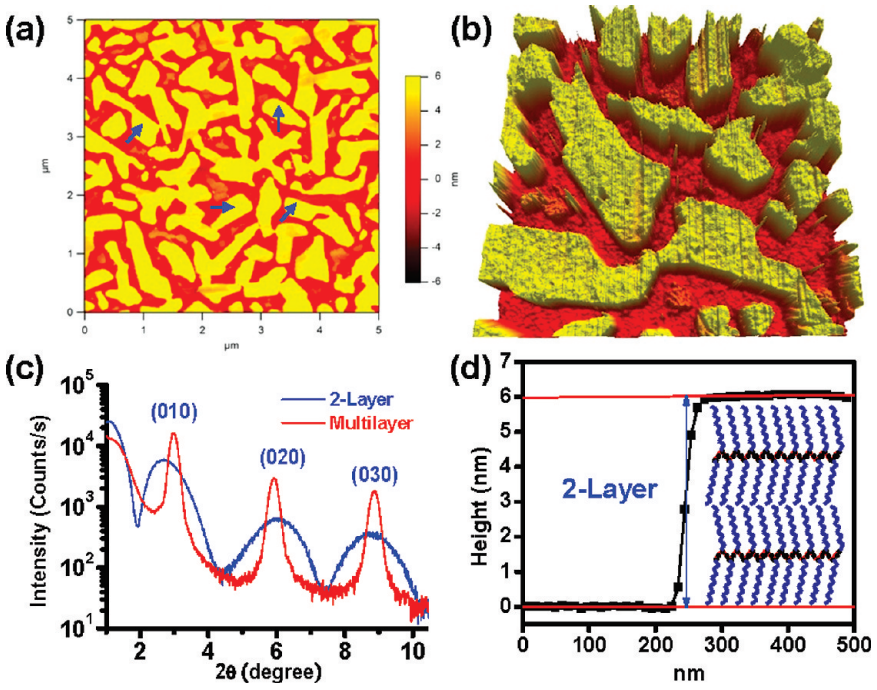

Figure 5. (a) Two-dimensional (5 μm × 5 μm) and (b) three-dimensional (2 μm × 2 μm) AFM micrographs of sample C, which is composed of nearly monodispersed (~95%) two-layer AgSC10 lamellar crystals. (c) Comparison of the X-ray diffractograms of samples C (blue curve) and M (red curve). (d) Average AFM line profile over 30 scans that cross from the substrate to the top surface of AgSC10 lamellae in sample C as annotated in panel a (the blue arrows). The step height equals the thickness of two-layer AgSC10 crystals.

the blue arrows in Figure 5a) that cross from the substrate to the top surface of the crystals are analyzed. Figure 5d shows an average over 30 line scans. The height scale has been corrected for the shift in baseline similar to the height histogram.

The FTIR spectrum (blue curve in Figure 1d) reveals that the peak positions of the d+ and d− modes are the same as those of multilayer samples and indicates high conformational order in the alkyl chains.

3.4. Monodispersed Single-Layer AgSC10 Lamellar Crystals. The AFM micrographs of sample E shown in Figure 6, parts a and b, indicate the presence of AgSC10 crystals of only one layer. As the number of layers in the multilayer AgSC10 crystals decreases the diffraction peaks become weaker and broader, as is evident in the case of nearly monodispersed two-layer AgSC10. Predictably, if the lamellae consist of only one single layer, the diffraction peaks vanish. Indeed, we do not observe the series of diffraction peaks in this single-layer sample.

However, we can use X-ray reflectivity to study the thickness of this single-layer structure. The experimental result is shown as the blue curve in Figure 6c. In order to evaluate this XRR result we use a molecular model for AgSC10 which consist of a −(Ag−S)− central network with alkyl chains extending on both sides (Figure 6c).[28,29,31] We obtain an excellent fit using this three-slab model as shown in Figure 6c. The top and bottom slabs of alkyl chains are 1.44 and 1.25 nm thick, respectively, and the central −(Ag−S)− network is 0.28 nm thick. The total thickness of this AgSC10 single layer is 2.97 ± 0.10 nm and is consistent with the layer spacing determined for multilayer crystals via XRD. AFM line scans (Figure 6e) that cross from the substrate to the top surface of the platelets are randomly selected on the entire sample surface, as annotated by the blue arrows in Figure 6a.

The surface coverage of the single-layer AgSC10 lamellar crystals in sample E is about 77% of the whole surface area. As expected, when the amount of Ag is decreased to smaller values (0.06 nm), we still obtain only single-layer AgSC10 crystals. Figure 7 compares AFM micrographs and height histograms of single-layer AgSC10 samples obtained by using different amounts of Ag. The amount of AgSC10 varies proportionally as well as the surface coverage on the substrate. It is also possible to produce single-layer AgSC10 with larger surface coverage by increasing the amount of Ag. However, this increases the possibility of the growth of AgSC10 crystals with more layers. Therefore, more delicate control on Ag distribution and annealing temperature would be required. The FTIR spectrum (red curve in Figure 1d) indicates high conformational order in the alkyl chains similar to the multilayer crystals. These single-layer lamellae grow into ultralarge crystals on carbon membranes as shown in Figure 6f, probably because of the easier transport of AgSC10 on carbon. Faceting is even more pronounced (up to 3 μm) in these samples.

4. DISCUSSION

4.1. Formation of AgSR Lamellar Crystals. The synthesis of AgSR crystals via the reaction between Ag clusters and alkanethiol vapor is consistent with our prior work on the reaction between Ag clusters and alkanethiol solution.[16] The advantage of utilizing alkanethiol vapor is that samples can be easily grown on a variety of substrates such as carbon membranes (on Cu grid) without the complications of liquid submersion, and this prevents the delamination of AgSR lamellae from the substrate due to the poor adhesion. In addition, the use of alkanethiol vapor also provides the capability of controlling the amount of alkanethiol that can reach the Ag clusters if the experiments are conducted in vacuum.

dx.doi.org/10.1021/ja107817x |J. Am. Chem. Soc. 2011, 133, 4367–4376

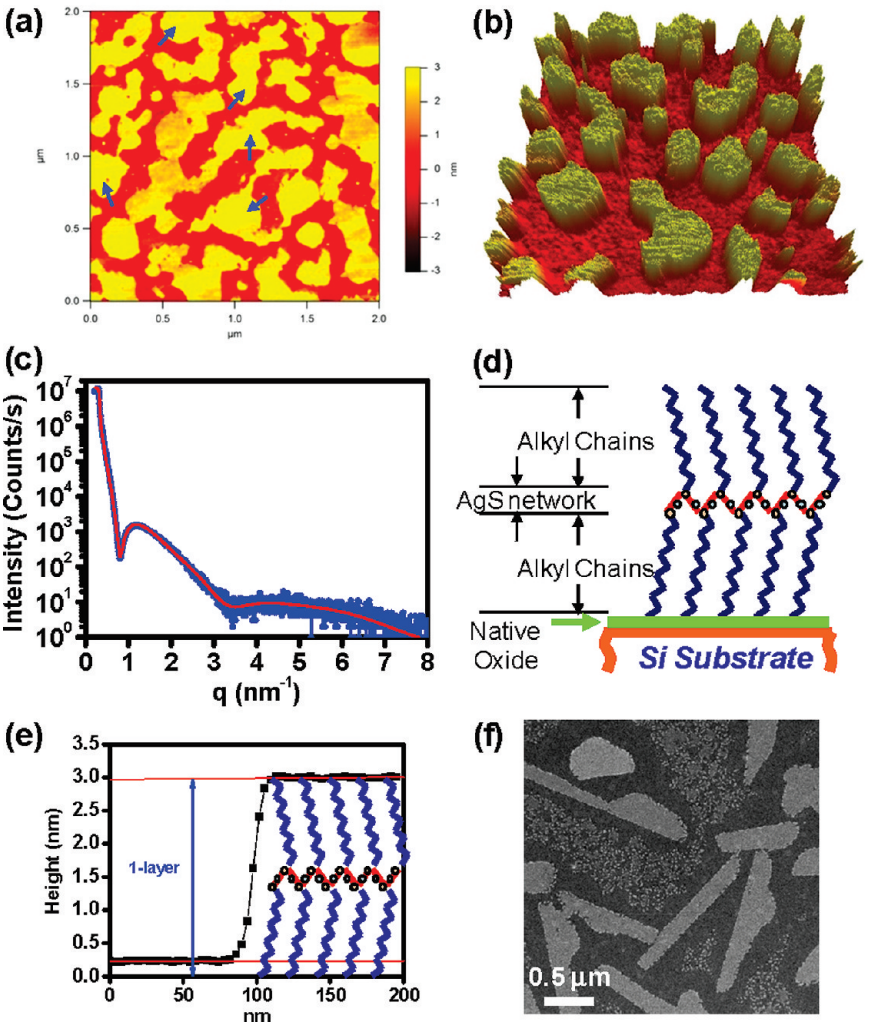

Figure 6. (a) Two-dimensional (2 μm × 2 μm) and (b) three-dimensional (2 μm × 2 μm) AFM micrographs of sample E, which is composed of uniform height single-layer AgSC10 lamellar crystals. (c) X-ray reflectivity measurement (blue curve) and simulation fitting (red curve) of the single-layer AgSC10 lamellae. (d) Schematic of the three-slab model for the XRR fitting of single-layer AgSC10. (e) Average AFM line profile over 60 scans that cross from the substrate to the top surface of AgSC10 lamellae in sample E as annotated in panel a (the blue arrows). The step height equals the thickness of single-layer AgSC10 crystals. (f) TEM micrographs of single-layer AgSC10 crystals.

The formation of AgSR can be explained by the instability of MPCs, which depends on the cluster size and the organic molecules. Starting from the Ag metallic clusters, the initial product in the reaction between Ag and alkanethiol would naturally be MPCs. However, the subsequent stages of the reaction involve the destruction of MPCs. Therefore, MPCs are considered as intermediate products in the formation of AgSR. This is in contrast to the observation that metal−thiolate is an intermediate product in the liquid-phase synthesis of MPCs.[14,15]

Walter et al. proposed that an MPC is composed of a metal core and a protective ligand shell, i.e., a core−shell structure.[3,25] The metal atoms in the core are still in the metallic state, whereas those in the shell are bonded with organic molecules and are oxidized. A stable MPC has (1) a compact, symmetric metal core; (2) an electron shell closing in the metal core; (3) a complete steric shielding of the ligand shell.[13] We suggest two possible paths for the formation of AgSR—the removal of Ag atoms from clusters and the collapse of MPCs.

First, since only the clusters with the core sizes satisfying the above requirements are stable, it is energetically preferred for the redundant Ag atoms to be removed from the clusters in the initial formed MPCs. In other words, besides forming protective monolayers on the Ag clusters, the alkanethiol also acts as an etchant. Conceivably, the Ag atoms that are removed from the clusters are involved in forming AgSR. Second, small MPCs can also transform into AgSR due to the steric instability. The alkyl chains in the MPCs are inclined to have a parallel packing due to the van der Waals interaction, especially for longer chains. On the other hand, the metal atoms in the cluster shell prefer the structure of the metal cores. Small cluster size further complicates the competition. Therefore, the large alkyl chain length (e.g., $C_{10}H_{21}$ in this study) and small cluster size weaken the stability of MPCs and promote the formation of AgSR.

4.2. Amount of Ag. Controlling the amount of Ag is critical in obtaining AgSR as the final reaction product. Small clusters are less stable in the presence of excess alkanethiol and are easier to be converted into AgSR phase, whereas large clusters have higher probability surviving the reaction as MPCs. Decreasing the amount of Ag increases the fraction of Ag incorporated in the AgSR phase. On the basis of the stoichiometry of the final

dx.doi.org/10.1021/ja107817x |J. Am. Chem. Soc. 2011, 133, 4367–4376

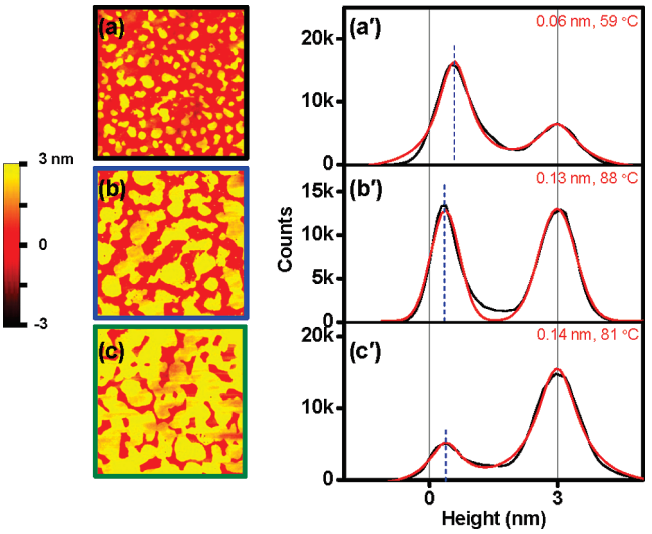

Figure 7. (a−c) AFM micrographs of samples G, E, and F, which are composed of different amounts (surface coverage) of single-layer AgSC10 lamellar crystals. (a′−c′) Height histograms corresponding to the micrographs in panels a−c. The experimental parameters (l_{Ag} and T_{Ann}) are listed in the top-right corner of each histogram.

products, when the diameter of the Ag clusters is below ~5 nm (0.5 nm Ag deposition), the majority (>90%) of the clusters are eventually consumed as AgSC10.

The amount of Ag also determines the minimum number of layers in AgSR crystals. For example, on the basis of the molecular model of AgSR,[31] the complete reaction between 0.18 nm of Ag and decanethiol vapor can generate a full-coverage single-layer AgSC10 on the surface. The corresponding area density of the alkyl chains is 1.77×10^{-9} mol/cm^2. Similarly, 0.18*n* nm of Ag on the surface can lead to the formation of a full-coverage *n*-layer AgSR single crystal. However, the AgSR is not one uniform single crystal and not always parallel to the substrate. The lateral dimension and orientation of AgSR crystals are compromised by the real surface condition. Subsequent thermal annealing promotes the growth of small crystals into large ones which are orientated in parallel with the substrate.

4.3. Crystal Growth: Ripening and Nucleation. The initial size of the AgSR depends on the size and spacing of Ag clusters. For example, single Ag clusters with a diameter of 2 nm produce (nucleate) single crystals of single-layer AgSR with diameters of 5.4 nm, which is smaller than the distance between the nearest-neighbor clusters. Therefore, each cluster acts as a closed system with regards to Ag. Growth of larger crystals is achieved through the lateral transport of AgSR on the surface and occurs in two directions—lateral and vertical—via two different processes: ripening and nucleation.

The lateral growth or ripening for a single layer is achieved via coalescence of adjacent grains and/or surface diffusion of AgSR segments. In contrast, the formation of additional layers (layer-building mode) requires epitaxial nucleation process on the basal planes of selected existing crystals. The kinetic barrier for the nucleation is higher than that of the ripening, and thus the nucleation requires a higher annealing temperature. This difference allows us to selectively decouple the two growth processes and to obtain specific layer thicknesses.

To synthesize small AgSR lamellar crystals with only one layer, we adjust the annealing temperature to promote ripening and suppress second-layer nucleation. The annealing temperature is critical to the thickness (number of layers) of the final products, since excessive annealing temperature creates crystals with large number of layers even though the cluster size may be small.

4.4. Comparison of AgSR, Alkane, and Polyethylene. AgSR typically exists in a multilayer structure—stacked layers. Similar to AgSR, polyethylene and short-chain alkanes have the same major components (alkyl chains) and also form stacked layers. Therefore, it is interesting to compare the multilayer structures of these three materials. In some aspects all of these multilayer systems are similar in that the layers stack regularly and thus should show long-range layer-by-layer order (e.g., diffraction patterns). However, one difference is the nature of the crystalline registration in between adjacent layers. Each layer of polyethylene has regions of folded chain segments at the basal surfaces which are characterized as amorphous.[49] Although the layers of large polyethylene crystals can be orientated with each other, no experimental proof shows that uniform local registration or epitaxy occurs at the interface of adjacent layers. In contrast, stacked-layer crystals of alkanes have ordered methyl groups as the terminating species at the basal surfaces (top and bottom) of each layer, which allows adjacent layers to be registered with one another.[50] We suggest that the AgSC10 layered system is more similar to the stacked-layer alkane system. Both have methyl groups as terminating species, and thus the registration between adjacent layers should be achievable. In addition, both AgSR and alkanes have more exact layer thickness defined by the length of alkyl chains. Further analysis using TEM, XRD, and calorimetry should be useful in determining the degree of registration between layers of AgSC10.

4.5. Correction of AFM Baseline. AFM provides information about the thickness of AgSC10 lamellar crystals which can further be used to derive the layer thickness and the number of layers. Two methods are used in this work to analyze the data—plotting height histograms and measuring step heights. In both methods, the substrate area (the open areas between AgSC10 crystals in the micrographs) is considered the baseline in the height axis. Ideally, the substrate area is clear of any materials and the baseline is zero, i.e., the substrate peak should be centered at zero in a height histogram. However, the substrate area is sometimes covered with residues such as unreacted decanethiol or lying-down AgSC10 segments which affect the accuracy of the measurement. For example, if no correction is made, the measured lamellar thicknesses would be slightly lower than the predicted values. In addition, the full width at half-maximum (fwhm) values of the substrate peaks (1.0−1.2 nm) in Figure 2a−e are about 2 times that of a bare Si substrate (0.5 nm) which has not be exposed to Ag or alkanethiol.

The amount of residue is reduced during thermal annealing in vacuum as the excess decanethiol desorbs and the AgSC10 segments transport and merge into large crystals. Figure 8 summarizes the deviation of the measured lamellar thicknesses from the theoretical values for samples A−E which is plotted versus the annealing temperature. The deviation decreases as the annealing temperature increases. However, high annealing temperature leads to epitaxial nucleation which creates crystals with a large number of layers. For example, the average number of layers in sample E would progressively increases to two and three layers if the samples are annealed to 95 and 110 °C, respectively. In order to synthesize AgSC10 with only one or two layers, the annealing temperature should be lower than 90 °C. Therefore, the residue effect is inevitable in characterizing the lamellar

dx.doi.org/10.1021/ja107817x |*J. Am. Chem. Soc.* 2011, 133, 4367–4376

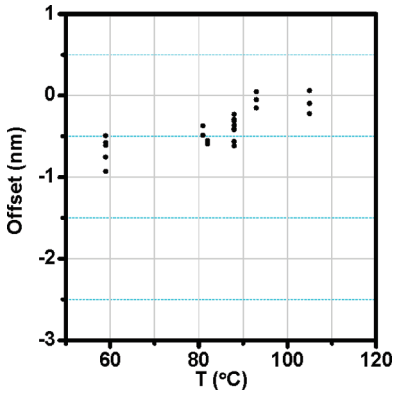

Figure 8. Difference between the measured and predicted values, plotted as a function of the annealing temperature.

thickness of AgSC10 crystals in this work using AFM, and thus the baseline correction is necessary. However, this residue effect does not interfere with XRD study. To fulfill the data correction, the height histograms are shifted (to larger heights) as demonstrated in Figure 2a−e, based on XRD and XRR values of layer spacing.

5. CONCLUSION

In summary, we developed a new synthesis method to produce metal−thiolate by reacting Ag clusters with alkanethiol vapor. Preferential formation of AgSR versus MPCs as the final reaction product is achieved by reducing the cluster size. The thickness of AgSR lamellae can be further manipulated and systematically reduced to a single layer by decreasing the amount of Ag and lowering the annealing temperature.

Single-layer AgSC10 lamellar crystals are produced by using 0.1 nm of Ag and annealing at 90 °C. These single-layer lamellae show the same attributes as multilayer crystals regarding layer thickness and conformation order. These single-layer lamellae are 2D crystals and are the thinnest form of AgSC10 just as graphene is the thinnest form of graphite. Other examples of organic 2D crystals include those synthesized using the Langmuir−Blodgett (LB) method.[51]

AUTHOR INFORMATION

Corresponding Author
l-allen9@illinois.edu

ACKNOWLEDGMENT

This work was supported by NSF-DMR-1006385 and NSF-DMR-0735286. Microanalysis characterization was carried out in part in the Frederick Seitz Materials Research Laboratory Central Facilities, University of Illinois, which are partially supported by the U.S. Department of Energy under Grants DE-FG02-07ER46453 and DE-FG02-07ER46471. The authors thank Professor P. Geil, Professor J.-M. Zuo, and Professor K.-C. Hsieh for discussion and suggestions and M. Sardela, S. MacLaren, C.-H. Lei, and D. Jeffers for their generous help. The authors also thank Dr. M. Green and Dr. D. Lavan at National Institute of Standards and Technology for disussions. The nanocalorimetry sensors were fabricated at the Cornell NanoScale Facility, a member of the National Nanotechnology Infrastructure Network, which is supported by the NSF-ECS-0335765.

REFERENCES

(1) Knight, W. D.; Clemenger, K.; Deheer, W. A.; Saunders, W. A.; Chou, M. Y.; Cohen, M. L. *Phys. Rev. Lett.* **1984**, *52*, 2141–2143.
(2) Efremov, M. Y.; Schiettekatte, F.; Zhang, M.; Olson, E. A.; Kwan, A. T.; Berry, R. S.; Allen, L. H. *Phys. Rev. Lett.* **2000**, *85*, 3560–3563.
(3) Jadzinsky, P. D.; Calero, G.; Ackerson, C. J.; Bushnell, D. A.; Kornberg, R. D. *Science* **2007**, *318*, 430–433.
(4) Smetana, A. B.; Klabunde, K. J.; Sorensen, C. M. *J. Colloid Interface Sci.* **2005**, *284*, 521–526.
(5) Geim, A. K.; Novoselov, K. S. *Nat. Mater.* **2007**, *6*, 183–191.
(6) DiBenedetto, S. A.; Facchetti, A.; Ratner, M. A.; Marks, T. J. *Adv. Mater.* **2009**, *21*, 1407–1433.
(7) Bachman, R. E.; Bodolosky-Bettis, S. A.; Glennon, S. C.; Sirchio, S. A. *J. Am. Chem. Soc.* **2000**, *122*, 7146–7147.
(8) Cha, S. H.; Kim, J. U.; Kim, K. H.; Lee, J. C. *Chem. Mater.* **2007**, *19*, 6297–6303.
(9) Bakr, O. M.; Amendola, V.; Aikens, C. M.; Wenseleers, W.; Li, R.; Dal Negro, L.; Schatz, G. C.; Stellacci, F. *Angew. Chem., Int. Ed.* **2009**, *48*, 5921–5926.
(10) Kind, M.; Woll, C. *Prog. Surf. Sci.* **2009**, *84*, 230–278.
(11) Gandhi, D. D.; Lane, M.; Zhou, Y.; Singh, A. P.; Nayak, S.; Tisch, U.; Eizenberg, M.; Ramanath, G. *Nature* **2007**, *447*, 299–302.
(12) Love, J. C.; Estroff, L. A.; Kriebel, J. K.; Nuzzo, R. G.; Whitesides, G. M. *Chem. Rev.* **2005**, *105*, 1103–1169.
(13) Cossaro, A.; Mazzarello, R.; Rousseau, R.; Casalis, L.; Verdini, A.; Kohlmeyer, A.; Floreano, L.; Scandolo, S.; Morgante, A.; Klein, M. L.; Scoles, G. *Science* **2008**, *321*, 943–946.
(14) Yee, C. K.; Jordan, R.; Ulman, A.; White, H.; King, A.; Rafailovich, M.; Sokolov, J. *Langmuir* **1999**, *15*, 3486–3491.
(15) Chen, S. W.; Templeton, A. C.; Murray, R. W. *Langmuir* **2000**, *16*, 3543–3548.
(16) Hu, L.; Zhang, Z. S.; Zhang, M.; Efremov, M. Y.; Olson, E. A.; de la Rama, L. P.; Kummamuru, R. K.; Allen, L. H. *Langmuir* **2009**, *25*, 9585–9595.
(17) Bain, C. D.; Troughton, E. B.; Tao, Y.; Evall, J.; Whitesides, G. M.; Nuzzo, R. G. *J. Am. Chem. Soc.* **1989**, *111*, 321–335.
(18) Laibinis, P. E.; Whitesides, G. M.; Allara, D. L.; Tao, Y. T.; Parikh, A. N.; Nuzzo, R. G. *J. Am. Chem. Soc.* **1991**, *113*, 7152–7167.
(19) Woodruff, D. P. *Phys. Chem. Chem. Phys.* **2008**, *10*, 7211–7221.
(20) Yu, M.; Bovet, N.; Satterley, C. J.; Bengio, S.; Lovelock, K. R. J.; Milligan, P. K.; Jones, R. G.; Woodruff, D. P.; Dhanak, V. *Phys. Rev. Lett.* **2006**, *97*, 166102.
(21) Gronbeck, H.; Hakkinen, H. *J. Phys. Chem. B* **2007**, *111*, 3325–3327.
(22) Gronbeck, H.; Hakkinen, H.; Whetten, R. L. *J. Phys. Chem. C* **2008**, *112*, 15940–15942.
(23) Mazzarello, R.; Cossaro, A.; Verdini, A.; Rousseau, R.; Casalis, L.; Danisman, M. F.; Floreano, L.; Scandolo, S.; Morgante, A.; Scoles, G. *Phys. Rev. Lett.* **2007**, *98*, 016102.
(24) Hakkinen, H.; Walter, M.; Gronbeck, H. *J. Phys. Chem. B* **2006**, *110*, 9927–9931.
(25) Walter, M.; Akola, J.; Lopez-Acevedo, O.; Jadzinsky, P. D.; Calero, G.; Ackerson, C. J.; Whetten, R. L.; Gronbeck, H.; Hakkinen, H. *Proc. Natl. Acad. Sci. U.S.A.* **2008**, *105*, 9157–9162.
(26) Gronbeck, H.; Walter, M.; Hakkinen, H. *J. Am. Chem. Soc.* **2006**, *128*, 10268–10275.
(27) Negishi, Y.; Nobusada, K.; Tsukuda, T. *J. Am. Chem. Soc.* **2005**, *127*, 5261–5270.
(28) Dance, I. G.; Fisher, K. J.; Banda, R. M. H.; Scudder, M. L. *Inorg. Chem.* **1991**, *30*, 183–187.
(29) Baena, M. J.; Espinet, P.; Lequerica, M. C.; Levelut, A. M. *J. Am. Chem. Soc.* **1992**, *114*, 4182–4185.

(30) Fijolek, H. G.; Grohal, J. R.; Sample, J. L.; Natan, M. J. *Inorg. Chem.* **1997**, *36*, 622–628.
(31) Bensebaa, F.; Ellis, T. H.; Kruus, E.; Voicu, R.; Zhou, Y. *Langmuir* **1998**, *14*, 6579–6587.
(32) Voicu, R.; Badia, A.; Morin, F.; Lennox, R. B.; Ellis, T. H. *Chem. Mater.* **2000**, *12*, 2646–2652.
(33) Voicu, R.; Badia, A.; Morin, F.; Lennox, R. B.; Ellis, T. H. *Chem. Mater.* **2001**, *13*, 2266–2271.
(34) Parikh, A. N.; Gillmor, S. D.; Beers, J. D.; Beardmore, K. M.; Cutts, R. W.; Swanson, B. I. *J. Phys. Chem. B* **1999**, *103*, 2850–2861.
(35) Bardeau, J. F.; Parikh, A. N.; Beers, J. D.; Swanson, B. I. *J. Phys. Chem. B* **2000**, *104*, 627–635.
(36) Dubois, L. H.; Zegarski, B. R.; Nuzzo, R. G. *J. Chem. Phys.* **1993**, *98*, 678–688.
(37) Olson, E. A.; Efremov, M. Y.; Zhang, M.; Zhang, Z. S.; Allen, L. H. *J. Microelectromech. Syst.* **2003**, *12*, 355–64.
(38) Efremov, M. Y.; Olson, E. A.; Zhang, M.; Schiettekatte, F.; Zhang, Z. S.; Allen, L. H. *Rev. Sci. Instrum.* **2004**, *75*, 179–191.
(39) Lai, S. L.; Guo, J. Y.; Petrova, V.; Ramanath, G.; Allen, L. H. *Phys. Rev. Lett.* **1996**, *77*, 99–102.
(40) Zhang, M.; Efremov, M. Y.; Schiettekatte, F.; Olson, E. A.; Kwan, A. T.; Lai, S. L.; Wisleder, T.; Greene, J. E.; Allen, L. H. *Phys. Rev. B* **2000**, *62*, 10548–10557.
(41) Efremov, M. Y.; Olson, E. A.; Zhang, M.; Zhang, Z.; Allen, L. H. *Phys. Rev. Lett.* **2003**, *91*, 085703.
(42) Mayer, M. Proceedings of the15th International Conference on the Application of Accelerators in Research and Industry, Denton, TX, 1999; Duggan, J. L., Stippec, B., Morgan, I. L., Eds.; American Institute of Physics, 1999; p 541.
(43) Zhang, Z. S.; Wilson, O. M.; Efremov, M. Y.; Olson, E. A.; Braun, P. V.; Senaratne, W.; Ober, C. K.; Zhang, M.; Allen, L. H. *Appl. Phys. Lett.* **2004**, *84*, 5198.
(44) Levchenko, A. A.; Yee, C. K.; Parikh, A. N.; Navrotsky, A. *Chem. Mater.* **2005**, *17*, 5428–5438.
(45) Terrill, R. H.; Postlethwaite, T. A.; Chen, C. H.; Poon, C. D.; Terzis, A.; Chen, A.; Hutchison, J. E.; Clark, M. P.; Wignall, G.; Londono, J. D.; Superfine, R.; Falvo, M.; Johnson, C. S., Jr.; Samulski, E. T.; Murray, R. W. *J. Am. Chem. Soc.* **1995**, *117*, 12537–12548.
(46) Badia, A.; Singh, S.; Demers, L.; Cuccia, L.; Brown, G. R.; Lennox, R. B. *Chem.—Eur. J.* **1996**, *2*, 359–363.
(47) Dorset, D. L. *Crystallography of the Polymethylene Chain: An Inquiry into the Structure of Waxes*; Oxford University Press: New York, 2005; Chapters 1−2.
(48) Dorset, D. L. Crystallography of the Polymethylene Chain: An Inquiry into the Structure of Waxes; Oxford University Press: New York, 2005.
(49) Weber, C. H. M.; Chiche, A.; Krausch, G.; Rosenfeldt, S.; Ballauff, M.; Harnau, L.; Gottker-Schnetmann, I.; Tong, Q.; Mecking, S. *Nano Lett.* **2007**, *7*, 2024–2029.
(50) Kitaigorodskii, A. I. *Organic Chemical Crystallography*; Consultants Bureau: New York, 1961.
(51) Schwartz, D. K. *Surf. Sci. Rep.* **1997**, *27*, 241–334.